12051

LiMn$_2$O$_4$ Nanorods, Nanothorn Microspheres, and Hollow Nanospheres as Enhanced Cathode Materials of Lithium Ion Battery

Jia-Yan Luo, Huan-Ming Xiong, and Yong-Yao Xia*

Department of Chemistry & Shanghai Key Laboratory of Molecular Catalysis and Innovative Materials, Fudan University, Shanghai, 200433, P. R. China

Nanostructured lithium intercalated compound has been demonstrated to be the most promising approach to improve the powder density of lithium ion batteries because of it providing a relatively short Li ion diffusion path. While the conventional nanostructured LiMn$_2$O$_4$, typically prepared at low temperatures, were almost all polycrystalline and low crystallinity, which would impair the stability of the crystallographic structure and charge−discharge cycling ability of LiMn$_2$O$_4$. In this paper, we systematically describe a topochemical method for successful synthesis of LiMn$_2$O$_4$ nanorods, nanothorn microspheres, and hollow nanospheres, and their electrochemical lithium insertion/desertion properties are extensively studied. We also investigated the effects of particle size, morphology, synthesis method, and crystal structure on the electrochemical properties of spinel LiMn$_2$O$_4$. The method described in the present work may assist in the design of novel nanostructured materials for application in a lithium ion battery.

1. Introduction

Li ion batteries, owing to their high energy density, lightweight, and long cycle life have widely used for consumer electronic devices. However, present Li ion technologies fall short of meeting the higher charge−discharge rate capability requirement of electric vehicles (EV), which was considered to relieve side issues linked to air pollution combined with the foreseen oil shortage. Since the demand for high performance exceeds the capabilities of the existing Li ion battery technology, electrode materials with superior properties and performance and low cost must be developed.[1–3]

Spinel LiMn$_2$O$_4$ with a three-dimensional crystal structure is at present a very prospective candidate as a cathode material of lithium ion batteries due to its low cost, acceptable environmental impact, and excellent voltage profile characteristics;[4,5] thus, the battery system based on LiMn$_2$O$_4$/carbon couple has been used commercially in many types of electronic equipment.[6] However, their power density is generally low because of a large polarization at high charge−discharge rates for the slow lithium diffusion in the solid active material.[7–10] Recently nanostructured lithium intercalated compounds with various morphologies have been extensively prepared to improve their rate capability for lithium ion batteries: for instance, nanoparticles (CoO, Li$_4$Ti$_5$O$_{12}$, LiMn$_2$O$_4$),[11–13] nanowires (Co$_3$O$_4$, TiO$_2$−B),[14–16] nanotubes (V$_2$O$_5$, LiMn$_2$O$_4$),[17–19] hollow spheres (V$_2$O$_5$, SnO$_2$, LiMn$_2$O$_4$)[20–22] and mesoporous materials (TiO$_2$−P$_2$O$_5$, Sn$_2$P$_2$O$_7$, V$_2$O$_5$, TiO$_2$−carbon nanotube)[23–27] and so on. Indeed, such an improvement is often considered to be achieved at the expense of high volumetric energy density, but high volumetric energy density and high power are often incompatible requirement. However, this is not always the case for high-rate use: because of the low diffusion coefficient in the solid phase (e.g., 10^{-10}–10^{-12} cm^2 s^{-1} for LiMn$_2$O$_4$), only the thin surface layer of the host material is available for Li ion insertion/extraction at high charge−discharge rates for bulk materials.

Most cathode materials for high-voltage lithium batteries were consisted of ternary or quaternary lithium transition-metal oxides, the synthesis of which required high-temperature treatments. These conditions increased the crystal growth rate and hindered the obtainment of nanostructured materials as a result. While the conventional nanostructured LiMn$_2$O$_4$, which were typically prepared at low temperatures, were almost all polycrystalline and low crystalline. It has been widely acknowledged that the high crystallinity would improve the stability of the crystallographic structure and charge−discharge cycling ability of LiMn$_2$O$_4$ by hindering Mn dissolution from the spinel material into the electrolyte.[28–30] Therefore, the discharge capacities, cycling life, and rate performance of rechargeable lithium ion batteries are dramatically affected by the particle size, surface morphology and synthesized method of the active materials constituting the cathodes. Thus, it is of great importance, but a challenge, to develop a facile and systematic method to synthesize various nanostructured spinel LiMn$_2$O$_4$ with high crystallinity.

Herein, we systematically report a topochemical method for the preparation of high crystalline spinel LiMn$_2$O$_4$ with representative morphology of 1D nanorods, 3D nanothorn microspheres, and 3D hollow nanospheres, because it has been reported that Li$^+$ ions and e$^-$ may be inserted into 1D nanowires synchronously, rendering them ionically and electronically conducting simultaneously;[15,16] while assembling randomly arranged 1D nanorods into 3D ordered nanothorn microspheres would facilitate the ion transportation and enhance the volumetric energy density; comparing to 1D nanowires, hollow nonospheres possess several different areas of contact between electrode material and electrolyte, i.e., the inner and the outer wall surfaces, as well as the nanopore channels.[20,31,32] Various nanostructured spinel LiMn$_2$O$_4$ were synthesized by air-calcining lithiated MnO$_2$ precursor at a low temperature of 550 °C, which was synthesized by chemical lithiation of various nanostructured MnO$_2$ with LiI at 70 °C for 12 h. The electrochemical lithium insertion/desertion properties of the three nanostructured LiMn$_2$O$_4$ were extensively investigated and compared.

* Corresponding author. Fax: (+86)-21-55664177. E-mail: yyxia@fudan.edu.cn.

Experimental Section

The synthesis of α-MnO$_2$ nanorods was carried out by a hydrothermal method on the basis of the previous work of Li's group.[33]

$$3MnSO_4 + 2KMnO_4 + 2H_2O \rightarrow$$
$$5\alpha-MnO_2 + K_2SO_4 + 2H_2SO_4$$

A mixture of 0.2 g of MnSO$_4$·H$_2$O and 0.5 g of KMnO$_4$ was placed in distilled water at room temperature to form a mixed solution, which was then transferred into a Teflon-lined stainless steel autoclave, sealed, and maintained at 140 °C for 12 h. After the reaction was complete, the resulting brownish-black solid product was filtered off, washed with distilled water and ethanol to remove ions possibly remaining in the final products, and finally dried at 100 °C in air.

The preparing of γ-MnO$_2$ nanothorn microspheres can be formulated as following:[34]

$$5MnSO_4 + 2KBrO_3 + 4H_2O \rightarrow$$
$$5\gamma-MnO_2 + Br_2 + K_2SO_4 + 4H_2SO_4$$
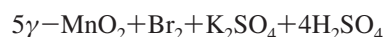
A 50 mL aqueous solution containing 2 mmol of MnSO$_4$ and 1 mmol of KBrO$_3$ was put in a flask and was stirred with a magnetic stirrer until a transparent solution was obtained. The solution was then transferred into a Teflon-lined stainless steel autoclave sealed and maintained at 110 °C for 16 h. The product was collected, washed and dried in a manner similar to that of the α-MnO$_2$ nanorods.
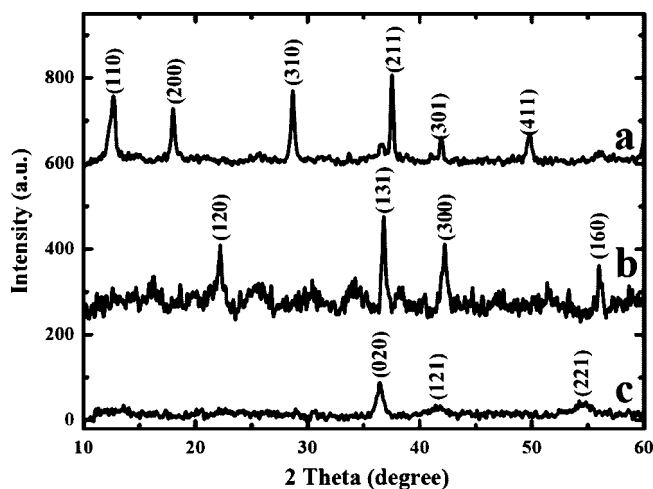
γ-MnO$_2$ hollow nanospheres were synthesized by a facile; template-free self-assembly process at room temperature in a short period according to a previous literature.[35]

$$3BaMnO_4 + 3H_2SO_4 \rightarrow 3BaSO_4 + MnO_2 + 2HMnO_4 + 2H_2O$$
$$2HMnO_4 + 2H_2O + 3MnSO_4 \rightarrow 5\gamma-MnO_2 + 3H_2SO_4$$

A 2.67 mL sample of 4.23 M H$_2$SO$_4$ was added dropwise to 100 mL of 0.1 M BaMnO$_4$. After being vigorously stirred at room temperature for 10 min, the solution was centrifuged and decanted. The resultant pink solution was added dropwise to 400 mL of 0.02 M MnSO$_4$ while being rapidly stirred for 12 h at room temperature. The slurry formed was filtered and washed with deionized water and ethanol and then dried in air at 100 °C for 12 h.

The spinel LiMn$_2$O$_4$ nanorods, nanothorn microspheres, and hollow nanospheres were prepared as follows with minor modification of our previous results:[36] A 0.1675 g sample of LiI was dissolved in 25 mL of acetonitrile and then stirred at room temperature until the solution became clear. Then 0.145 g of as-prepared various nanostructured MnO$_2$ precursors were added into the solution. The suspension was heated to 70 °C and kept under reflux for 12 h, Centrifugated, washed several times with acetonitrile, and dried under vacuum at 200 °C for 1 day. The final products were obtained by calcinations the lithiated samples in a muffle stove at the temperature of 550 °C for 2 h at a heating rate of 2 °C/min in air.

Powder XRD measurements were performed on a Rigaku D/MAX-IIA X-ray diffractometer using Cu Kα radiation. SEM images were obtained on Philip XL30 operated at 25 kV. TEM was performed using a JEOL JEM-2010 electron microscope. Nitrogen adsorption−desorption measurements were performed on a Micromeritics Tristar 3000 system at 77 K. The chemical composition of the final product was conducted by inductively coupled plasma (ICP) analysis. The manganese valence in LiMn$_2$O$_4$ was calculated by analysis according Kozawa's

Figure 1. XRD patterns of the as-synthesized (a) α-MnO$_2$ nanorods, (b) orthorhombic γ-MnO$_2$ nanothorn microspheres, and (c) hexagonal γ-MnO$_2$ hollow nanospheres.

method.[37] The oxidation of manganese can be determined by titrating the excess FeSO$_4$ solution with standard KMnO$_4$ solution.

Electrochemical measurements were carried out in CR2016-type coin cell with lithium metal as negative electrode. The working electrode was fabricated by compressing a mixture of the active materials, conductive material (acetylene black (AB)), and binder (polytetrafluoroethylene (PTFE)) in a weight ratio of LiMn$_2$O$_4$/AB/PTFE = 85:10:5 onto an aluminum grid at 10 Mpa. The electrodes were punched in the form of disks typically with a diameter of 12 mm and weight of about 10 mg and then dried at 120 °C for 12 h. The cell assembly was operated in a glovebox filled with pure argon. The electrolyte solution was 1 M LiPF$_6$/ethylene carbonate (EC)/propylene carbonate (PC)/diethyl carbonate (DEC) (1:1:1 by volume). The cell was galvanostatically cycled between 3−4.3 V vs Li/Li$^+$ at various current densities at 25 °C. Lithium insertion into LiMn$_2$O$_4$ electrode was referred to as discharge and extraction as charge.

Results and Discussion

Composition of the Products. The crystal phase of the as-prepared MnO$_2$ samples was analyzed by powder X-ray diffraction. X-ray powder patterns of the three as-prepared compounds were shown in Figures 1 and 2. All the diffraction peaks in Figure 1a can be indexed to a pure tetragonal phase of α-MnO$_2$ (JCPDS 44−0141).[33] The XRD patterns in Figure 1b can be ascribed to orthorhombic γ-MnO$_2$ (JCPDS 14−644),[34] and the XRD patterns in Figure 1c correlated to hexagonal γ-MnO$_2$ (a space group for this structure is not applicable due to the combination of different tunnel geometries).[35] The sharp, intense XRD peaks of the obtained α-MnO$_2$ products indicated its better crystallinity, while the much broader, less intensity diffraction indicated that the crystallinity of orthorhombic and hexagonal γ-MnO$_2$ was not as good as that of α-MnO$_2$.

For the heat-treated lithiated MnO$_2$, all the diffraction peaks of the three XRD patterns can be indexed to a pure face-centered cubic [space group: $Fd\bar{3}m$ (no. 227)] LiMn$_2$O$_4$, which was in good agreement with that reported previously,[38–40] thus demonstrating the single-phase of the three as-synthesized spinel LiMn$_2$O$_4$. Furthermore, it could be observed that there was no distinct different in peak position of the three products. Whereas the peak intensity rather differed from one to another, a broadening of the peaks was owned to the smaller grain size.

Enhanced Cathode Materials

J. Phys. Chem. C, Vol. 112, No. 31, 2008 **12053**
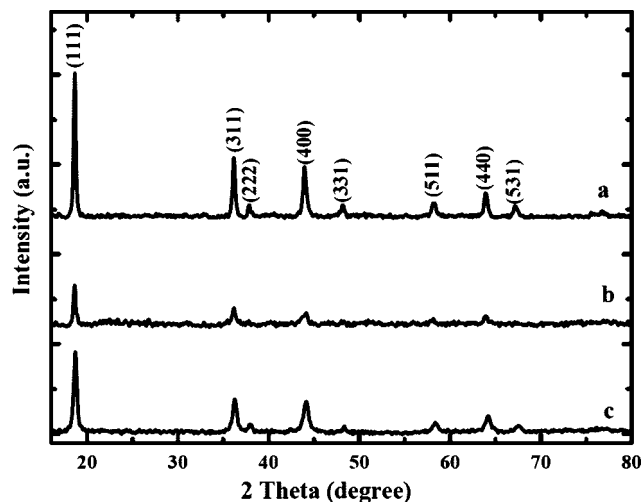
Figure 2. XRD patterns of the as-synthesized $LiMn_2O_4$ (a) nanorods, (b) nanothorn microspheres, and (c) hollow nanospheres.

From the powder X-ray diffraction patterns, we can calculate the crystallite size for each sample according to Scherrer's method. The crystallite size of the products was estimated from the (111) peaks. One could deduce that a crystallite dimension of about 29 nm for the $LiMn_2O_4$ nanorods, while about 22 and 20 nm for the $LiMn_2O_4$ hollow nanospheres and nanotrorn microspheres, respectively.

Morphology of the Products. The morphology and structure of the MnO_2 precursors and the $LiMn_2O_4$ products were then examined by scanning electron microscope (SEM), a transmission electron microscope (TEM), and selected-area electrode diffraction (SAED) at an acceleration voltage of 200 kV. As shown in Figure 3, parts A and B, the α-MnO_2 nanorods had diameters of 80−100 nm and lengths from 2 to 5 um. To convert the MnO_2 to $LiMn_2O_4$, the MnO_2 nanorods were lithiated by LiI, and then calcined at 550 °C for 2 h in air. The TEM image in Figure 3, parts C and D, showed that, after lithiation and calcinations at 550 °C, the nanorods retained their morphology, indicating their excellent thermal stability. The corresponding selected-area electrode diffraction (SAED) pattern (Figure 3E, inset) taken from a single $LiMn_2O_4$ nanorod, in which the spots (marked with white spots) with strong intensity, could be indexed to a cubic phase, indicating high crystalline nature of a bulk sample. The high-resolution TEM (HRTEM) image of the long nanorod in Figure 3F confirmed a well-defined high crystalline structure. Defects in this structure were apparent, as an amorphous phase close to the outside surface of the nanorods.

Figure 4A was an overall morphology of the orthorhombic γ-MnO_2, which indicated that the obtained product consisted of large nanothorn microspheres with a diameter of about 4−8 um. The magnified SEM image shown in Figure 4B clearly displayed that the orthorhombicγ-MnO_2 nanorods attached together and were assembled into 3D nanothorn nanostructures with rod-like crystallites radiating from the center. The TEM image in Figure 4, parts C and D, showed that, after lithiation and calcinations at 550 °C, the nanothorn nanostructures retained their morphology, with the tip of nanorods been transfigured slightly. Close observation as shown in Figure 4, parts E and F revealed that the individual $LiMn_2O_4$ nanorods were straight and have relatively uniform diameters of about 80 nm with an average length about 2−3 um. More details of the structure of the nanothorn microspheres $LiMn_2O_4$ were investigated by the SAED pattern (inset of Figure 4G) and HRTEM, which indicates the high crystalline of the whole product.
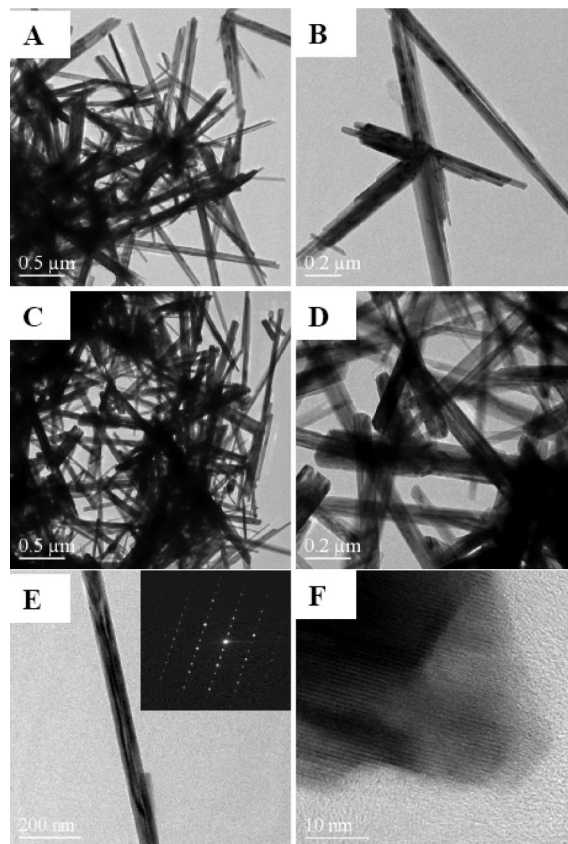
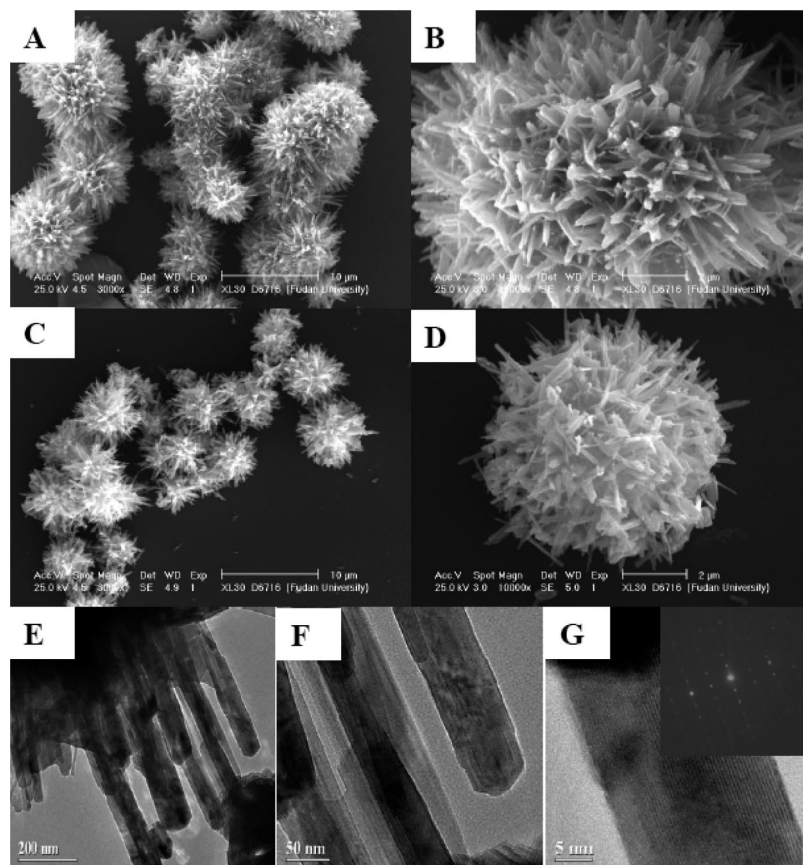**Figure 3.** (A, B) TEM images of the MnO_2 nanorods. (C−F) TEM images of the $LiMn_2O_4$ nanorods. The inset of panel E is the corresponding SEAD pattern of the MnO_2 nanorods.

Figure 5A showed a SEM image of the γ-MnO_2 hollow spheres. The sample mainly contained uniform nanospheres with diameter of about 500 nm and a rough surface. A TEM image (Figure 5B) showed the produced nanospheres were composed of a hollow inner cavity and thin outer shell. Further evidence for the shell structure could be found from other TEM images shown in Figure 5, parts C and D. The thickness of the nanosphere walls was ca. 50 nm, and the mesopores in the wall could be observed clearly. Figure 5E showed a panoramic SEM image of the as-synthesized $LiMn_2O_4$. As seen from Figure 5, parts E−G, the hollow spherical morphology remained almost the same after lithiation and calcinations. Representative HR-TEM taken near the edge along the wall of the nanospheres was shown in Figure 5, parts H and I. As seen from the images, the building units of the particular $LiMn_2O_4$ hollow nanospheres were structurally uniform single crystal, though we do not rule out the possibility of some point defects such as oxygen vacancies and manganese vacancies. The upper right inset in Figure 5G showed the corresponding SAED pattern from the hollow nanosphere without specimen tilting, indicating that they were structurally uniform high crystalline.

The specific BET surface areas and particle sizes of the three as-synthesized nanostructured $LiMn_2O_4$ were shown in Table 1. The surfaces areas of the obtained nanostructured $LiMn_2O_4$ were much lower that those of the MnO_2 precursor, due to the pore shrink and higher density after the heat-treatment. Nevertheless, these values were still higher than that of the corresponding solid state reaction counterpart. Moreover, the particle sizes were much smaller. It has been demonstrated that a large surface area could lead to an increase in the active materials/electrolyte reaction area, and the nanostructured

Figure 4. (A, B) SEM images of the MnO$_2$ nanothorn microspheres. (C, D) SEM images of the LiMn$_2$O$_4$ nanothorn microspheres. (E, F, G) TEM image of the LiMn$_2$O$_4$ nanothorn microspheres. The inset of panel G is the corresponding SEAD pattern of the MnO$_2$ nanothorn microspheres.
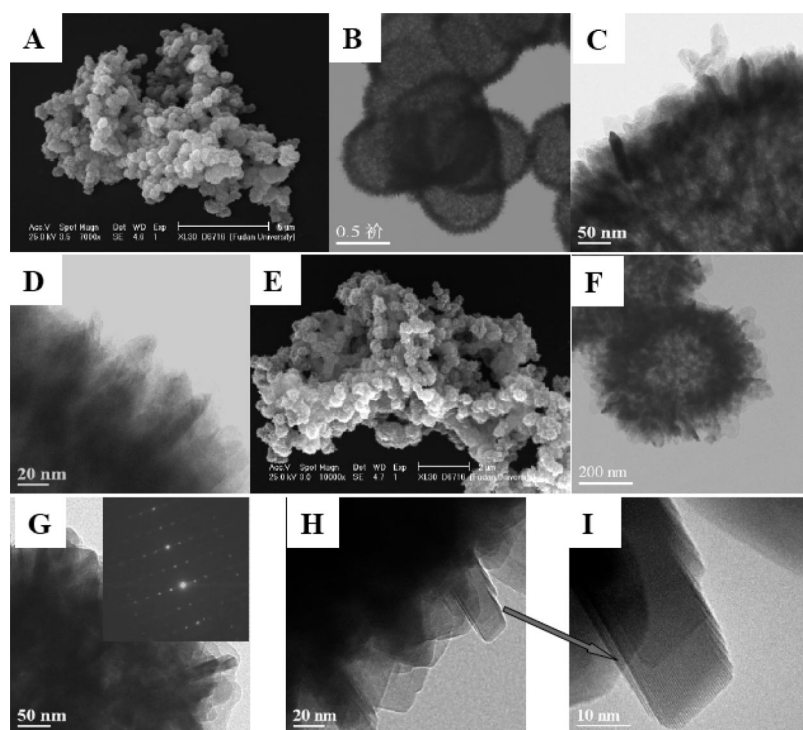
Figure 5. (A) SEM images of the MnO$_2$ hollow nanospheres. (B−D) TEM images of the MnO$_2$ hollow nanospheres. (E) SEM images of the LiMn$_2$O$_4$ hollow nanospheres. (F−I) TEM images of the LiMn$_2$O$_4$ hollow nanospheres. The inset of panel G is the corresponding SEAD pattern of the MnO$_2$ hollow nanospheres.

materials may facilitate the electrochemical insertion/extraction of lithium ion. As a result, a greatly improved electrochemical performance of the three as-synthesized nanostructured LiMn$_2$O$_4$ would be expected.

Electrochemical Performance. The typical galvanostatic charge−discharge behaviors of the three as-synthesized nanostructured LiMn$_2$O$_4$ recorded over the potential range between 3.0 and 4.3 V at the 0.1C rate (where C corresponds to complete

Enhanced Cathode Materials

J. Phys. Chem. C, Vol. 112, No. 31, 2008 **12055**

TABLE 1: Specific BET Surface Areas and Particle Sizes of the Three As-Synthesized Nanostructured $LiMn_2O_4$ and BET Surface Areas of MnO_2

	nanorods	nanothorn microspheres	hollow nanospheres
MnO_2, BET (m^2/g)	43	9	132
$LiMn_2O_4$, BET (m^2/g)	19	4	30
$LiMn_2O_4$, particle size along [111] direction, D (nm)	29	20	22

discharge in 1 h) were shown in Figure 6. The charge−discharge curves of the $LiMn_2O_4$ nanorods and nanothorn microspheres both presented two patent plateaus, with the discharge plateau one at 4.1 V and the other at 3.95 V. The appearance of the former plateau might because of the coexistence of λ-MnO_2−$Li_{0.5}Mn_2O_4$, while the latter was due to the coexistence of two pseudophases in the form of $Li_{0.5}Mn_2O_4$−$LiMn_2O_4$. The $LiMn_2O_4$ hollow nanospheres, however, presented two undistinguished plateaus with lower capacity, denoting the charge/discharge signature of the lithium-rich spinel,[39,40] which was generally expected to have better cycle performance as a cathode eletrode material than the normal stoichiometric one.
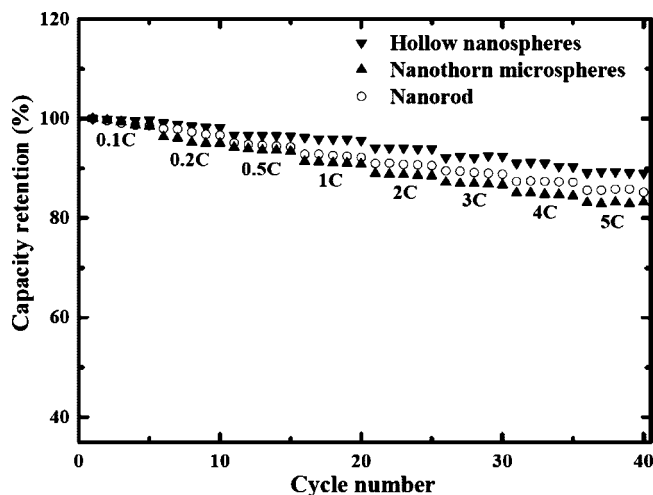
The chemical compositions of the as-prepared three nanostructured $LiMn_2O_4$ were analyzed by ICP, and it was found that the determination was $Li_{1.00}Mn_2O_4$ for nanorods, $Li_{1.02}Mn_2O_4$ for nanothorn microspheres, and $Li_{1.05}Mn_2O_4$ for hollow nanospheres, which accorded with the result of charge−discharge measurement.

To understand why the accommodation of Li^+ in the three different nanostructured MnO_2 results in the formation of spinel phase with variable Li/Mn ratio under the same synthetic condition, we should first consider the different arrangement of the MnO_6 octahedra in the two polymorphs of α-MnO_2 and γ-MnO_2 as presented in Figure 7. The α-MnO_2 presents in nature in several form such as Hollandite ($BaMn_8O_{16}$) and cryptomelane (KMn_8O_{16}). The structure of α-MnO_2 is consisted
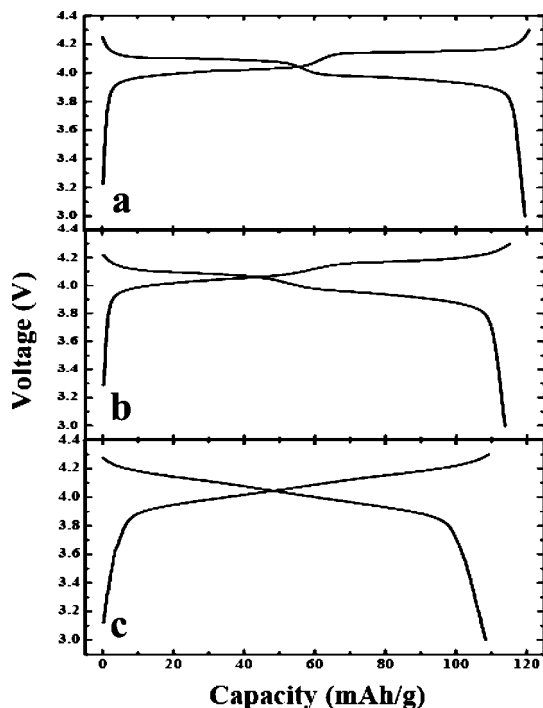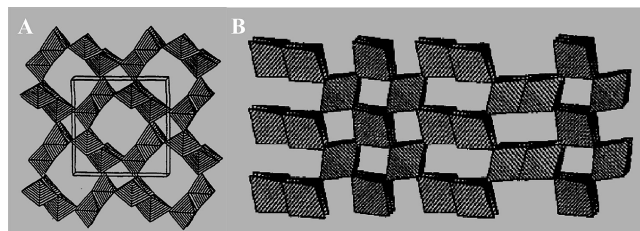
Figure 7. Structures of (A) α-MnO_2 and (B) γ-MnO_2 down the c axis.
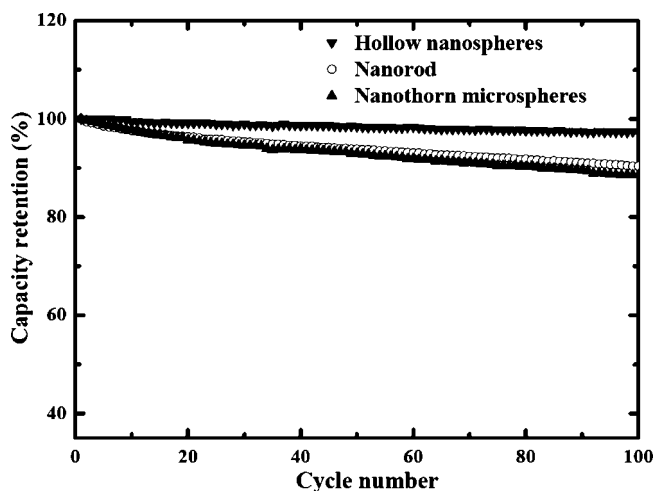
Figure 8. Variation of discharge capacity versus cycle number for the $LiMn_2O_4$ nanorods, nanothorn microspheres and hollow nanospheres electrodes between voltage limits of 3.0 and 4.3 V at the $1C$ rate.

of interlinking double chain of MnO_6 octahedra and an interstitial space comprised of one-dimensional channels of relative dimensions (2×2) and (1×1) that extend in a direction parallel to the c axis of a tetragonal unit cell (Figure 7A). The Ba^{2+} and K^+ cations or H_2O molecular reside in the center of (2×2) channels and provide stability to the structure. However, the present of these can impede the diffusion of Li^+ within the α-MnO_2 framework, thus hamper the accommodation of Li^+. While the structure of γ-MnO_2 is a randomly arranged combination of strips forming one-dimensional channels with a cross section corresponding to one and two octahedra, β-MnO_2 domains of relative size (1×1) and ramsdellite-MnO_2 domains of size (1×2), respectively (Figure 7B). Unlike α-MnO_2, γ-MnO_2 contains water which is located at grain boundaries and occluded within the structure. Moreover, the ramsdellite-MnO_2 can accommodate Li^+ up to a high lever without destruction of its structure.[41–49] So the Li/Mn ratio is generally higher in γ-MnO_2 than in α-MnO_2 during the lithiation of MnO_2 with LiI. Regarding $Li_{1.02}Mn_2O_4$ for nanothorn microspheres and $Li_{1.05}Mn_2O_4$ for hollow nanospheres, we speculate that the much higher surface area of γ-MnO_2 hollow nanospheres (132 m^2/g) than that of γ-MnO_2 nanothorn microspheres (9 m^2/g) may facilitate the lithiation of MnO_2 with LiI, thus lead to more lithium content in the γ-MnO_2 hollow nanospheres.

Figure 8 showed the cycle performance of the three as-synthesized nanostructured $LiMn_2O_4$ electrodes between potential limits of 3.0 and 4.3 V at the 1 C rate. The $LiMn_2O_4$ hollow nanospheres behaved a quite slow capacity fading on cycling with an average capacity loss of 0.02 $mAhg^{-1}$ per cycle during 100 charge−discharge cycles, in other words, the discharge capacity of the $LiMn_2O_4$ hollow nanospheres maintained above 98% of its initial capacity. While for $LiMn_2O_4$ nanothorn microspheres and nanorods, capacity retention of only

Figure 6. Typical charge/discharge curves of the $LiMn_2O_4$ (a) nanorods, (b) nanothorn microspheres and (c) hollow nanospheres electrodes between voltage limits of 3.0 and 4.3 V at the $0.1C$ rate.

Figure 9. Variation of discharge capacity versus cycle number for the LiMn$_2$O$_4$ nanorods, nanothorn microspheres and hollow nanospheres electrodes cycled at various rates between voltage limits of 3.0 and 4.3 V.

88% and 90% could be obtained within 100 charge/discharge cycles, respectively, indicating that better cycle performance was expected for the cell with a lithium-rich manganese oxide as a positive electrode than that with a normal spinel. Even that, the cycling reversibility of the as-synthesized LiMn$_2$O$_4$ nanorods and LiMn$_2$O$_4$ urchin-like nanostructures was better than that of many other reported nanostructured spinel LiMn$_2$O$_4$.[18,50,51] For example, only 69% of its initial capacity was maitained for the LiMn$_2$O$_4$ nanotubes, owning to its relatively low crystallinity.[18] The excellent cycling ability of the three as-synthesized nanostructured LiMn$_2$O$_4$ electrodes could be attributed to that the high crystallinity would improve the stability of crystallographic structure of the as-synthesized LiMn$_2$O$_4$, as well as the interspace among these nanostructures would act as a buffer layer to alleviate the volume expansion of the electrode during electrochemical insertion/extraction of lithium ion.

The rate performance especially the high rate discharge performance is another important aspect for the application of Mn-based spinel cathodes for EV/HEV power sources besides the cycling performance. Rates of up to 5C of the three as-synthesized nanostructured LiMn$_2$O$_4$ electrodes have been investigated and the results are shown in Figure 9. The cell was first cycled at 0.1C then, after some 5 cycles, the rate was increased in stages to 5C. In particular, about 89%, 85%, and 83% of the reversible capacity at 0.1C rate can be discharged at 5C rate for the LiMn$_2$O$_4$ hollow nanospheres, nanorods, and nanothorn microspheres, respectively. Thus the LiMn$_2$O$_4$ hollow nanospheres showed a better charge−discharge capability at higher current densities than that of the LiMn$_2$O$_4$ nanorods, and nanothorn microspheres. Nevertheless, these rate capabilities for the three as-synthesized nanostructured LiMn$_2$O$_4$ electrodes were much higher than the rate capability for the solid-state reaction spinel LiMn$_2$O$_4$, as well as that of most reported results for the spinel fabricated by techniques such as a sol−gel precipitation, Pechini process, electrochemical process, and template method.[13,18,50–53] Therefore, the results obtained above confirmed that the method described here could be employed as a rational route to synthesize high rate spinel LiMn$_2$O$_4$ with various nanostructures. The large capacity performance at high charge−discharge rate condition could be attributed to that the larger specific surface area of these materials would lead to higher current density and the small particle size could reduces

the lithium ion diffusion path, as well as the high crystallinity would improve the stability of crystallographic structure.

Conclusion

In summary, we have developed a topochemical method for successful synthesis of various nanostructured spinel LiMn$_2$O$_4$ with high crystallinity. The high crystallinity of the as-synthesized LiMn$_2$O$_4$ would improve the stability of crystallographic structure during cycling, and the interspace among these nanostructures would act as a buffer layer to alleviate the volume expansion of the electrode during electrochemical insertion/extraction of lithium ion, these would lead to better cycling ability of LiMn$_2$O$_4$. The larger specific surface area of these nanostructured materials will lead to higher current density and the small particle size can reduces the lithium ion diffusion path, thus better rate capability can be obtained. This topochemical method would address the problem that conventional method to synthesize nanostructured LiMn$_2$O$_4$ usually confronted: fast capacity fading due to the low crystallinity nanostructured LiMn$_2$O$_4$ typically prepared at low temperatures. And the topochemical method described in the present work could be used to synthesize various nanostructured LiMn$_2$O$_4$ such as nanorod, nanothorn microspheres and hollow nanospheres, by emplying various nanostructured MnO$_2$ precursor, and this method may assist in the design of novel nanostructured materials for the application in lithium ion battery. Furthermore, the strategy presents a new possibility for the synthesis of various nanostructured mixed metal oxides.

References and Notes

(1) Tarascon, J. M.; Armand, M. *Nature* **2001**, *414*, 359.
(2) Scrosati, B. *Nature* **1995**, *373*, 557.
(3) Nelson, R. F. *J. Power Sources.* **2001**, *92*, 2.
(4) Park, H. S.; Hwang, S. J.; Choy, J. H. *J. Phys. Chem. B* **2001**, *105*, 4860.
(5) Kovacheva, D.; Gadjov, H.; Petrov, K.; Mandal, S.; Lazarraga, M. G.; Pascual, L.; Amarilla, J. M.; Rojas, R. M.; Herrero, P.; Rojo, J. M. *J. Mater.Chem.* **2002**, *12*, 1184.
(6) Whittingham, M. S. *Chem. Rev.* **2004**, *104*, 4271.
(7) Yu, L. H.; Yang, H. X.; Ai, X. P.; Cao, Y. L. *J. Phys. Chem. B* **2005**, *109*, 1148.
(8) Wang, Y.; Takahashi, K.; Shang, H. M.; Cao, G. Z. *J. Phys. Chem. B* **2005**, *109*, 3085.
(9) Jiao, F.; Shaju, K. M.; Bruce, P. G. *Angew. Chem., Int. Ed.* **2005**, *44*, 6550.
(10) Arico, A. S.; Bruce, P. G.; Scrosati, B.; Tarascon, J. M.; Schalkwijk, V. *Nat. Mater.* **2005**, *4*, 366.
(11) Poizot, P.; Laruelle, S.; Grugeon, S.; Dupont, L.; Tarascon, J. M. *Nature* **2000**, *407*, 496.
(12) Doi, T.; Iriyama, Y.; Abe, T.; Ogumi, Z. *Chem. Mater.* **2005**, *17*, 1580.
(13) Curtis, C. J.; Wang, J. X.; Schulz, D. L. *J. Elctrochem. Soc.* **2004**, *151*, A590.
(14) Nam, K. N.; Kim, D. W.; Yoo, P. J.; Chiang, C. Y.; Meethong, N.; Hammond, P.; Chiang, Y. M.; Belcher, A. M. *Science* **2006**, *312*, 885.
(15) Armstrong, A. R.; Armstrong, G.; Canales, J.; Bruce, P. G. *Angew. Chem., Int. Ed.* **2004**, *43*, 2286.
(16) Armstrong, A. R.; Armstrong, G.; Canales, J.; Garcia, R.; Bruce, P. G. *Adv. Mater.* **2006**, *16*, 1133.
(17) Li, C. N. C.; Patrissi, J.; Che, G. L.; Martin, C. R. *J. Elctrochem. Soc.* **2000**, *147*, 2044.
(18) Li, X. X.; Cheng, F. Y.; Guo, B.; Chen, J. *J. Phys. Chem. B* **2005**, *109*, 14017.
(19) Wang, Y.; Takahashi, K.; Lee, K.; Cao, G. Z. *Adv. Func. Mater.* **2005**, *17*, 862.

Enhanced Cathode Materials

J. Phys. Chem. C, Vol. 112, No. 31, 2008 **12057**

(20) Cao, A. M.; Hu, J. S.; Liang, H. P.; Wan, L. J. *Angew. Chem., Int. Ed.* **2005**, *44*, 4391.

(21) Han, S.; Jang, B.; Kim, T.; Oh, S. M.; Hyeon, T. *Adv. Funct. Mater.* **2005**, *15*, 1845.

(22) Luo, J. Y.; Cheng, L.; Xia, Y. Y. *Electrochem. Commun.* **2007**, *9*, 1404.

(23) Zhou, H. S.; Lin, D. L.; Honma, I. *Nat. Mater.* **2004**, *3*, 65.

(24) Zhou, H. S.; Lin, D. L.; Hibino, M.; Honma, I. *Angew. Chem., Int. Ed.* **2005**, *44*, 797.

(25) Kim, E.; Son, D.; Kim, T. C.; Cho, J.; Park, B.; Ryu, K. S.; Chang, S. H. *Angew. Chem., Int. Ed.* **2004**, *43*, 5987.

(26) Liu, P.; Lee, S. H.; Tracy, C. E.; Yan, Y. F.; Turner, J. A. *Adv. Mater.* **2002**, *14*, 27.

(27) Moriguchi, I.; Hidaka, R.; Yamada, H.; Kudo, T.; Murakami, H.; Nakashima, N. *Adv. Mater.* **2006**, *18*, 69.

(28) Blyr, A.; Sigala, C.; Amatucci, G.; Guymard, D.; Chabre, Y.; Tarascon, J. M. *J. Elctrochem. Soc.* **1998**, *145*, 194.

(29) Gao, Y.; Dahn, J. R. *J. Elctrochem. Soc.* **1996**, *143*, 100.

(30) Kanamura, K.; Dokko, K.; Kaizawa, T. *J. Elctrochem. Soc.* **2005**, *152*, A391.

(31) Lou, X. W.; Wang, Y.; Yuan, C. L.; Lee, J. Y.; Archer, L. A. *Adv. Mater.* **2006**, *18*, 2325.

(32) Han, S. J.; Jang, B. C.; Kin, T.; Oh, S. M.; Hyeon, T. *Adv. Funct. Mater.* **2005**, *15*, 1845.

(33) Wang, X.; Li, Y. D. *Chem. Commun.* **2002**, 764.

(34) Wu, C. Z.; Xie, Y.; Wang, D.; Yang, J.; Li, T. W. *J. Phys. Chem. B* **2003**, *107*, 13583.

(35) Yuan, J. K.; Laubernds, K.; Zhang, Q. H.; Suib, S. L. *J. Am. Chem. Soc.* **2003**, *125*, 4966.

(36) Luo, J. Y.; Li, X. L.; Xia, Y. Y. *Electrochim. Acta* **2007**, *52*, 4525.

(37) Kozawa, A. *Memo. Fac. Eng. Nogoya Univ* **1959**, *11*, 243.

(38) Xia, Y. Y.; Zhou, Y. H.; Yoshio, M. *J. Elctrochem. Soc.* **1997**, *144*, 2593.

(39) Xia, Y. Y.; Yoshio, M. *J. Elctrochem. Soc.* **1997**, *144*, 4186.

(40) Xia, Y. Y.; Sakai, T.; Fujieda, T.; Yang, X. Q.; Sun, X.; Ma, Z. F.; McBreen, J.; Yoshio, M. *J. Elctrochem. Soc.* **2001**, *148*, A723.

(41) Thackeray, M. M.; Rossouw, M. H.; Kock, A.; Harpe, A. P. *J. Power Sources* **1993**, *43−44*, 289.

(42) Thackeray, M. M. *Mater. Res. Bull.* **1983**, *18*, 461.

(43) Thackeray, M. M. *Prog. Solid State Chem.* **1997**, *25*, 1.

(44) Gummow, R. J.; Kock, A.; Thackeray, M. M. *Solid State Ionics* **1994**, *69*, 59.

(45) Tarascon, J. M.; Guyomard, D. *Electrochim. Acta* **1993**, *38*, 1221.

(46) Xu, J. J.; Jain, G.; Yang, J. S. *Electrochem. Solid-State Lett.* **1993**, *5*, A152.

(47) Zhu, S. M.; Zhou, H. S.; Hibino, M.; Honma, I.; Ichihara, M. *Adv. Funct. Mater.* **2005**, *15*, 381.

(48) Armstrong, A. R.; Bruce, P. G. *Nature* **1996**, *381*, 499.

(49) Curtis, C. J.; Wang, J. X.; Schulz, D. L. *J. Elctrochem. Soc.,* **2004**, *151*, A590.

(50) Huang, Y. D.; Li, J.; Jia, D. Z. *J. Nanopart. Res.* **2004**, *6*, 533.

(51) Zhou, Y. K.; Shen, C. M.; Huang, J.; Lin, H. L. *Mater. Sc. Eng. B* **2002**, *95*, 77.

(52) Zhang, Y. L.; Shin, H. C.; Dong, J.; Liu, M. L. *Solid State Ionics* **2004**, *171*, 25.

(53) Skapin, A. S.; Gaberscek, M.; Dominko, R.; Bele, M.; Drofenik, J.; Jamnik, J. *Solid State Ionics* **2004**, *167*, 229.